Journal of
Applied and Computational Mechanics

Research Paper

Optimum Design of Nano-Scaled Beam Using the Social Spider Optimization (SSO) Algorithm

Büşra Uzun[1] , **Ömer Civalek[2]** , **Ibrahim Aydogdu[3]**

[1] Department of Civil Engineering, Faculty of Engineering, UludağUniversity, Bursa, Turkey, Email: buzun@uludag.edu.tr

[2] Research Center for Interneural Computing, China Medical University, Taiwan, Email: civalek@yahoo.com

[3] Department of Civil Engineering, Faculty of Engineering, Akdeniz University, Antalya, 07050, Turkey, Email: aydogdu@akdeniz.edu.tr

Abstract. In this research study, the optimum cross-sectional dimensions of nano-scale beam elements are investigated under different load conditions. Euler-Bernoulli beam model based on nonlocal elasticity theory is utilized for the analysis of the beam. Two types of nano-scaled beams are modeled; carbon nanotubes (CNTs) and Boron nitride nanotubes (BNNTs). The novel meta-heuristic based optimization algorithm called Social Spider Optimization (SSO) algorithm is employed to find the beam designs with the objective of minimizing the cross-sectional area. Furthermore, the obtained optimum cross-sectional dimensions, critical stress and displacement values of the beams are compared according to the material type, beam length, and load conditions.

1. Introduction

In recent technological studies, obtained products have become more durable and useful than the previous ones. This can be told as a result of nanotechnology [1,2]. In this study, the Euler-Bernoulli beam model based non-local elasticity theory is developed for the deflection Analysis of cantilever and simply supported beam and two types of nano-scaled beams are modeled; carbon nanotubes (CNTs) and Boron nitride nanotube (BNNT). Lately, there has been a lot of research on nonlocal continuum theory for modeling nanobeams [3–13]. In addition to nonlocal continuum theory, other theories are used for the analysis of ultra small-scaled structures. Akgöz and Civalek [14] presented the buckling response of axially loaded microbeams via modified couple stress and strain gradient elasticity theories. Also, Akgöz and Civalek [15] investigated the bending and vibration behavior of simply supported microbeams based on modified strain gradient theory. Sedighi [16] presented a size-dependent dynamic pull-in instability of vibrating electrically actuated micro beams in conjunction with the strain gradient elasticity theory. Electromechanical bending, buckling, and free vibration analyses of functionally graded piezoelectric nanobeams were presented by Beni [17] on the basis of the Euler-Bernoulli beam and couple stress theories. Samani and Beni [18] examined thermo-mechanical buckling analysis of the flexoelectric nanobeam based on the modified strain gradient theory. Esmaeili and Beni [19] investigated the size-dependent buckling and vibration behavior of functionally graded flexoelectric nanobeam with simply support and clamped-clamped boundary conditions. Ebrahimi and Barati [20] presented the vibration frequencies of an axially preloaded flexoelectric nanobeam subjected to the in-plane magnetic field in conjunction with nonlocal elasticity and surface elasticity theories. In addition, these studies, some papers about the behaviors of nanostructures with non-classical elasticity theories can be found in [21-27].

Minimizing the cross-sectional dimensions of the nano-scaled beams is essential to reduce their occupied areas. In the meantime, these structures have to resist external loads. Construction of balance between resistance and the

minimum cross-section is not an easy task due to handling a lot of possibilities and conditions. Optimization methods are excellent tools to handle this task. Depside having the ability to use in many design problems, classical optimization methods cannot be used complicated engineering design problems. Nature-Inspired optimization techniques are efficient tools to solve these design problems [28–31]. Social Spider Optimization (SSO) Algorithm is one of the novel addition to Nature-Inspired which mimics the behavior of social spider colonies [32,33]. Depside of being novelty, SSO algorithm is utilized for the solution of many problems such as mathematical functions [34,35,36], economic dispatch of thermal power unit [36], the penetration of plug-in electric vehicles [37], the non-convex economic load dispatch problem [38], design of steel space structures [39], design of support Vector Machines applied for energy theft detection [40] and CO2 and cost optimization of reinforced concrete columns [41]. Although the SSO algorithm is used in many optimization problems, the algorithm has not been applied to CNTs and BNNTs yet. Some, key papers on nanoscaled analyze have been listed in the literature [43,44].

In the study, a computer program has been developed to find the optimum cross-sectional dimensions of nano-scale beam elements. A novel and efficient optimization algorithm called the SSO algorithm was used in the program. The developed program optimized Seventy-two different nano-scale beams. Obtained optimum cross-section areas, maximum stress values, and maximum displacement values were discussed to test the efficiency of the algorithm and to investigate the variation of the optimum designs.

The remainder of this manuscript is organized as follows; In Section 2, the non-local elasticity theory is outlined. In Section 3, the non-local deflection theory is depicted for Euler-Bernoulli Beams. In Section 4, the optimization problem and SSO are identified in detail. Section 5 proposes design problems. Also, a set of results obtained from optimum designs for numerical solutions of the examples are presented and discussed in this section. Finally, concluding remarks are provided in Section 6.

2. Nonlocal Elasticity Theory

A classical elasticity theory which is used for the design of the structures under mechanical loads is not valid entirely for micro and especially for nanostructures. Obtained results lose their proximity to reality. Characteristic inner dimension effects of the micro materials could be considered as the most valid cause of this situation.

In other words, materials show quantum behaviors as their dimensions decrease. Consequently, the need for non-local elasticity theory emerged as the materials with brand new physical, chemical and biological properties begin to appear in these dimensions. Another situation differs from the classical theories is the increase in the importance of stress and displacement states of the points which are neighboring to relevant points in every point of the microstructure. Nonlocal elasticity theory depends on this statement [8,9].

Nonlocal elasticity theory is based on the concept that when stress on some point is calculated, it isn't enough to consider the displacement on that specific point; rather displacement on all other points must be taken on the account. When the object translates, some irregularities form in the shape of the object. As a result of these irregularities, some internal stress forms inside the object. For example; when some materials are deformed, the internal stress and deformation converge to infinity. If the solutions are made with non-local elasticity theory, these problem disappears [10]. As stated by Eringen [11], the linear theory of non-local elasticity leads to a set of integropartial differential equations for the displacements field for homogeneous, isotropic bodies. According to the non-local elasticity theory of Eringen's, the stress at any reference point in the body depends not only on the trains at this point but also on strains at all points of the body. This definition of the Eringen's nonlocal elasticity is based on the atomic theory of lattice dynamics and some experimental observations on phonon dispersion. In this theory, the fundamental equations involve spatial integrals which represent weighted averages of the contributions of related strain tensor at the related point in the body. Thus theory introduces the small length scale effect through a spatial integral constitutive relation. For homogenous and isotropic elastic solids, the linear theory of nonlocal elasticity is described by the following equations [11]:

$$\sigma_{ij} + \rho\left(f_j - \ddot{u}_j\right) = 0 \tag{1a}$$

$$\varepsilon_{ij} = \frac{1}{2}\left(u_{ij} + u_{ji}\right) \tag{1b}$$

$$\sigma_{ij} = \int_V C_{klmn}\left(x - x'\right)\mathrm{d}V\left(x'\right) \tag{1c}$$

In the Eq. (1a); σ_{ij}, ρ, f_j and $\ddot{u}_j$ represent respectively nonlocal stress, mass density, mass force and second-order derivative of displacement. In the Eq. (1b), ε_{ij} represents nonlocal displacement. In the Eq. (1c) that is, the constitutive equation, x represents the position and C_{klmn} is the fourth-order elasticity tensor which is a function of $(x - x')$, and lastly V is the volume of the object. Double-notation index is given as:

$$u_{ij} = \frac{\partial u_i}{\partial u_j} \tag{2}$$

Stress tensor of isotropic objects and the form of this for isotropic objects is as follows:

$$\sigma_{ij}(x') = \int_V \alpha\left(|x'-x|\right)\sigma_{ij}^c(x')\,\mathrm{d}V(x') \tag{3a}$$

$$\sigma_{ij}^c(x') = \lambda\varepsilon_{rr}\sigma_{ij} + 2\mu\varepsilon_{ij} \tag{3b}$$

here $\sigma_{ij}^c(x')$ represents the classical stress, $\alpha(|x'-x|)$ is the distance in Euclidean form, λ and μ are Lamé constants. Distance in the Euclidean form is given as:

$$L_0\alpha\left(|x'-x|,\varphi\right) = \delta\left(|x'-x|\right) \tag{4}$$

This relation specifies the constituent equation of the nonlocal theory. Here, $\delta(|x'-x|)$ is the Dirac function. L_0 is the linear differential operator and φ is a material constant. Accordingly,

$$L_0 = 1 - l^2\varphi^2\nabla^2 \tag{5a}$$

$$\varphi = e_0\frac{a}{l} \tag{5b}$$

where a represents the characteristic internal length and l represents the characteristic outer length. Eq. (5b) is shown more clearly below:

$$L_0\sigma_{ij} = \sigma_{ij}^c \tag{6}$$

The most fundamental stress equation of nonlocal elasticity theory Eq. (9) is obtained by firstly substituting Eq (5b) expression into Eq. (5a), and after that substituting the resulting expression into Eq. (6):

$$\left(1 - \mu\frac{\partial^2}{\partial x^2}\right)\sigma_{xx} = E\varepsilon_{xx} \tag{7}$$

Here μ is defined as $\mu = (e_0 a)^2$ and it is called as nonlocal parameter.

3. Nonlocal Deflection of Euler–Bernoulli Beams

If the two sides of the stress equation seen in Eq. (6) are multiplied by the transverse coordinate y, and then it is integrated over the field, Eq. (7) is obtained.

$$\left(1 - \mu\frac{\partial^2}{\partial x^2}\right)\int_A \sigma_{xx}y\,\mathrm{d}A = \int_A \sigma_{ij}^c y\,\mathrm{d}A \tag{8}$$

As a result of equilibrium equations, the expressions below are established:

$$\int_A \sigma_{xx}y\,\mathrm{d}A = M_{xx}, \qquad \int_A \sigma_{ij}^c y\,\mathrm{d}A = M^c = -EI\frac{\partial^2 w}{\partial x^2} \tag{9}$$

Here M_{xx} is the nonlocal internal moment effect and M^c is the classical internal moment effect. Nonlocal moment equals the opposite sign of the distributed load is:

$$q - \mu\frac{\partial^2 q}{\partial x^2} = EI\frac{\partial^4 w}{\partial x^4} \tag{10}$$

In the classical formulations, z parameter represents the longitudinal coordinate. However, in order to avoid interfering with the coordinate of the nonlocal internal affect location, the representation of the longitudinal coordinate is changed to x. The nonlocal deflection equation is only applied for a beam simply supported from each end and with homogenous distributed loading condition. For this situation, the relevant analytical equation is obtained, but in the results section, no numeric data is presented. This situation is planned to be handled in future studies.

When both sides of Eq. (10) are integrated four times in a row according to the longitudinal coordinate, as presented below [12]:

$$w(x) = \frac{1}{EI}\left(\frac{q}{24}x^4 + \frac{c_1}{6}x^3 + \frac{c_2}{2}x^2 + c_3 x + c_4 - \frac{\mu q}{2}x^2 \right) \tag{11}$$

To define integration constants, boundary conditions should be used. But it should be noted that boundary conditions are not similar to classical conditions. Atomic parameters also affect the conditions. Namely, if the expressions in the Eq. (12) are substituted into Eq. (10), Eq. (14) is obtained:

$$M_{xx} - \mu \frac{\partial^2 M_{xx}}{\partial x^2} = -EI \frac{\partial^2 w}{\partial x^2} \tag{12}$$

where the relation between nonlocal internal moment affect and distributed load substituted in place, and nonlocal internal moment affect left at the left side of the equation:

$$M_{xx} = -EI \frac{\partial^2 w}{\partial x^2} - \mu q \tag{13}$$

When this expression substituted into Eq. (13) and rearranged, the moment expression is attained:

$$M_{xx} = -\frac{q}{2}x^2 - c_1 x - c_2 \tag{14}$$

After that, the application of boundary conditions could be executed. These boundary conditions are listed below:

$$v(0) = 0 \tag{15a}$$

$$M_{xx}(0) = 0 \tag{15b}$$

$$v(L) = 0 \tag{15c}$$

$$M_{xx}(L) = 0 \tag{15d}$$

Firstly, the condition Eq. (15a) is applied, and $c_4 = 0$ is obtained. Then, the condition Eq. (15b) is applied and $c_2 = 0$ is obtained. When condition Eq. (15d) is applied:

$$c_1 = -\frac{qL}{2} \tag{16}$$

is obtained. Lastly, when condition Eq. (15c) is implemented:

$$c_3 = \frac{qL^3}{24} + \frac{\mu q L}{2} \tag{17}$$

is obtained [9]. Finally, when all numeric results for integration constants are substituted into Eq. (13), nonlocal deflection equation is obtained:

$$w(x) = \frac{1}{EI}\left(\frac{q}{24}x^4 - \frac{qL}{12}x^3 - \frac{\mu q}{2}x^2 + \left(\frac{qL^3}{24} + \frac{\mu q L}{2} \right)x \right) \tag{18}$$

The geometric characteristics of curves, whether classical or non-local, do not change. For example, the displacements at the endpoints are equal and zero, and the maximum deflection occurs in the nonlocal solution, as in the classical, at the midpoint. However, nonlocal maximum deflection and classical maximum deflection are not equal due to the presence of atomic parameters. If $x = L/2$, we can easily obtain:

$$w = \frac{1}{EI}\left(\frac{5qL^4}{384} + \frac{\mu q L^2}{8} \right) \tag{19}$$

The most important interpretation to be made here is atomic parameters increase the value of classical deflection. Thus, it is understood that maximum stress and bending moment values also increase. Consequently, in design optimizations to be made according to the classical and nonlocal solution of a bending element, it can be said that the nonlocal solution will require a more cross-sectional area than the classic.

4. Optimization of Nano–Scaled Beams

4.1 Optimization Problem

In this study, the cross-section of bending elements with different loading and supporting conditions will be determined with respect to stress and displacement limits. Therefore, the objective function is the cross-section.

$$A(b,h) = b \cdot h \tag{20a}$$

$$A(D) = \frac{\pi D^2}{4} \tag{20b}$$

here, b, h and D parameters respectively represent; widths of the rectangular cross-section, the height of the rectangular cross-section, and the diameter of the circular cross-section. These parameters are also defined as the design variables of the optimization problem which is represented as " $\vec{\mathbf{x}}$ ". The optimization problem will be carried out with two different boundary conditions. These are displacement and stress boundary conditions and their limiting functions are as follows:

$$S_\sigma\left(\vec{\mathbf{x}}\right) = \frac{\sigma_{max}}{\sigma_{limit}} - 1 \leq 0 \tag{21a}$$

$$S_w\left(\vec{\mathbf{x}}\right) = \frac{w_{max}}{w_{limit}} - 1 \leq 0 \tag{21b}$$

here, σ_{max} and σ_{limit} are respectively maximum and boundary stress, w_{max} and w_{limit} are maximum and boundary deflection. If the beam design does not satisfy the limitation functions, its objective function value is penalized according to the following formula:

$$A_p = A \cdot (1 + C)^2 \tag{22}$$

where C is total violation value which is calculated as follows:

$$C = c_\sigma + c_w, \quad c_\sigma = \begin{cases} 0 & \text{for} \quad S_\sigma\left(\vec{\mathbf{x}}\right) \leq 0 \\ S_\sigma\left(\vec{\mathbf{x}}\right) & \text{for} \quad S_\sigma\left(\vec{\mathbf{x}}\right) > 0 \end{cases}, \quad c_w = \begin{cases} 0 & \text{for} \quad S_w\left(\vec{\mathbf{x}}\right) \leq 0 \\ S_w\left(\vec{\mathbf{x}}\right) & \text{for} \quad S_w\left(\vec{\mathbf{x}}\right) > 0 \end{cases} \tag{23}$$

Performance of the beam design (Per) is inversely proportional to its penalized objective function value which is described as follows:

$$\text{Per} = \frac{1}{A_p} \tag{24}$$

4.2 Social Spider Optimization (SSO)

Social Spider Optimization method which is the novel nature-inspired optimization method is proposed by Cuevas et al. in the year 2014. The method is developed based on the hive behavior of the spiders in nature. In this method, a certain number of female and male social spiders generate a social hive.

For each spider, different evolutionary operators like vibration, movement, and coupling are used based on gender and performance. Social spiders perform these social operators inside the interaction area that is called a common spider web. Firstly, the social hive is created on the common web. After that, social spiders vibrate in order to communicate with each other. Because of this vibration spiders move towards each other and the movement ratio depends on the vibration intensity [28,29].

After the completion of the vibration operator, spiders perform the other operator, which is coupling on their new position. After the completion of this operator, a new spider is obtained, the results are compared with the data of the worst social spider, if the new spider is better, then the worst spider is alienated from the hive and coupling solution, in other words, the new spider enters the hive. In the meantime, the alienated spider and new spider are the same genders. These operations are iterated in the specified number of times in the program and the detection of the best social spider becomes the solution of the optimization problem [28,29].

The SSO algorithm uses two main search parameters called colony size (CS) and the female inclination factor (PF). In the algorithm, each spider represents one beam design (candidate solution), and the algorithm cannot assign the spider to more than one beam at the same time. During the optimization process, CS beams designs and their objective function values are stored in the algorithm memory. Each coordinate of the spider position represents the dimensions of the beam cross-section. Movement of the spider means the modification of the beam design in the algorithm memory. The

generation of a new spider after coupling means the production of a candidate beam design using available solutions in the algorithm memory. According to these definitions, the steps of the SSO algorithm are described below:

Step 1: The SSO algorithm defines the number of female (N_f) and male (N_m) individuals by using the following formula:

$$N_f = int\left[(0.9 - 0.25 \cdot rnd) \cdot CS\right] \tag{25}$$

$$N_m = N_s - N_f \tag{26}$$

where rnd is a random number generated in an interval between 0 and 1, int is a mathematical function which coverts real value to an integer value.

Step 2: The algorithm generates initial solutions randomly according to the following formula:

$$X_{ij} = lb_j + \left(ub_j - lb_j\right) \cdot rnd , \quad i = 1, ..., CS , \quad j = 1, ..., ndv \tag{27}$$

In this equation, X, lb, ub, i, j, and ndv terms respectively represent current solution pool available in the algorithm memory, lower and upper limits of the design variables, the subscripts of the spider and the design variable. Then, the initial solutions are evaluated, and their performance values are calculated using formulas given in section 4.1.

Step 3: The algorithm assigns the first N_f solutions to female spiders. The females change their positions according to vibrations received from the nearest (vb_n) and the best (having the best performance value) (vb_b) spiders. In other words, the beam designs assigned to the female spiders are updated using the following formula:

For $rnd \leq PF$

$$X_{i,j}^{new} = X_{i,j} + rnd \cdot Vb_{i,n} \cdot \left(X_{c,j} - X_{i,j}\right) + rnd \cdot Vb_{i,b} \cdot \left(X_{b,j} - X_{i,j}\right) + rnd\left(rnd - 0.5\right)$$

$$\tag{28}$$

For $rand \leq PF$

$$X_{i,j}^{new} = X_{i,j} - rnd \cdot Vb_{i,n} \cdot \left(X_{c,j} - X_{i,j}\right) - rnd \cdot Vb_{i,b} \cdot \left(X_{b,j} - X_{i,j}\right) + rnd\left(rnd - 0.5\right)$$

$i = 1, .., N_f , \quad j = 1, .., ndv$

where i, c and b terms are indexes of the current female, nearest spider to i^{th} female spider, the best spider in the colony. Vibrations values received from the opponent spiders depend on weight on opponent spider (w_i) and distance between the spiders. The algorithm calculates vibration values as follows:

$$Vb_{i,j} = \begin{cases} w_j \cdot e^{-d_{ij}^2} & \text{for} \quad w_j \geq w_i \\ 0 & \text{for} \quad w_j < w_i \end{cases} \tag{29}$$

where w_j is the weight of the spider which receives the vibration, d_{ij} is Euclidean distance between the spiders. Calculation of the d_{ij} value is described as follows:

$$Vb_{i,j} = \sqrt{\sum_{k=1}^{ndv} \left(X_{i,k} - X_{j,k}\right)^2} \tag{30}$$

The weight of each spider depends on its performance of its assigned solution (Per_i). The weight of each spider is calculated using the following formula:

$$w_i = \frac{Per_i - Per_{worst}}{Per_{best} - Per_{worst}} , \quad i = 1, ..., CS \tag{31}$$

In the above equation, Per_{best} and, Per_{worst} terms respectively represent performance values of best and worst solutions in the algorithm memory.

Step 4: The algorithm assigns the remaining solution to male spiders. Then male spiders are divided into two groups called dominant and nondominant spiders. If the weight of the male spider is greater than the median weight of the male spiders, the algorithm defines the male spider as dominant. Otherwise, the male spider is determined as

nondominant male spiders. Then, spiders use movement operators. In other words, the beam designs assigned to the dominant and nondominant male spiders are updated using the following formula according to the following equation.

For dominant spiders

$$X_{i,j}^{new} = X_{i,j} + rnd \cdot Vibf_i \cdot \left(X_{f,j} - X_{i,j} \right) + rnd \left(rnd - 0.5 \right)$$

For nondominant spiders

$$X_{i,j}^{new} = X_{i,j} + rnd \cdot \left(\frac{\sum\limits_{k=N_f+1}^{CS} X_{k,j} \cdot w_k}{\sum\limits_{k=N_f+1}^{CS} w_k} - X_{i,j} \right)$$
(32)

$i = 1, .., N_f , \quad j = 1, .., ndv$

Step 5: The coupling operator is performed in this step. First, the algorithm calculates the radius of the dominant male spider's active region to mate female spiders as follows:

$$r = \frac{\sum\limits_{j=1}^{ndv} \left(ub_j - lb_j \right)}{2 \cdot ndv}$$
(33)

If the Euclidean distance between the female spider and the dominant male spider (d_{ij}), the female spider is considered to be within the active region of the male spider. In this way, female spiders in the active area of all dominant male spiders are detected. After the detection process, attractiveness ratios (*AR*) of involved members (female spiders and dominant male spider) in the active region are calculated as follows:

$$AR_i = \frac{w_i}{\sum\limits_{j \in E} w_j}$$
(34)

where *E* represents the set of members in the active region. Then, design variables of the beam designs assigned to the most suitable individuals are selected according to *AR* values. The algorithm uses the stochastic based method called the roulette wheel technique for the selection. After the selection process, a new beam design is generated and assigned to the new spider. The performance of the new spider is better than the worst spider; the new spider replaces the worst spider.

Step 6: The performances of the displaced spiders are recalculated and the algorithm memory is updated. Then, stopping criteria reaching the maximum iteration number is controlled. If the criteria are carried out, the algorithm on, otherwise, the algorithm returns to step 3.

4.3 Sensitivity Analysis for the SSO Algorithm

The SSO method contains stochastic operations as other nature-inspired optimization techniques. Therefore, the performance of the SSO algorithm most depends on search parameters and sensitivity analysis is needed to determine the most suitable search parameters. In the literature, some researchers have carried out a sensitivity analysis for the problems having different sizes and types [6,12]. According to these studies, the internal search parameters are as follows: (*NS*=100, *PF*=0.5) for SSO.

5. Results

In numerical analysis, the selected cross-section types are rectangular and circular forms. The height of the rectangular cross-section for the minimum dimension is $h_{min} = 1\ nm$, and for the maximum dimension is $h_{max} = 7.5\ nm$, the width of the rectangular cross-section for the minimum dimension is $b_{min} = 0.5\ nm$ and for the maximum dimension is $b_{max} = 4.5\ nm$. The minimum dimension of the circular cross-section is $D_{min} = 0.5\ nm$ and the maximum dimension is $D_{max} = 6.5\ nm$. The beam spans range from $L_{min} = 10\ nm$ to $L_{max} = 100\ nm$.

The selected cross-section type and dimension parameters of this section will be optimized under static loads. The CNT and BNNT stress limiters to be used in the optimization problem are defined as $\sigma_{limit}^{CNT} = 11\ GPa$ and $\sigma_{limit}^{BNNT} = 11\ GPa$.

As a displacement limiter, the beam length is defined as $w_{limit} = L/200$ [42].

When micro and nanoscale structures are modeled, micrometer and nanometer units are used. Therefore, it is convenient to use the units of *nm* and nN/nm^2 for displacement and stress parameters for nanoscale structures.

Likewise, the elasticity module must be selected accordingly. Otherwise, applied loads like *10 tons*, *100 N/m* which are

encountered frequently in the mechanical analysis of macro structures yields to extreme stresses and displacements. This is called the perception effect of unchanged quantity. In order to prevent this situation, the numerical values to be used in the nano-sized units should be quite small [42].

Static loads to be used in this study are as follows:

For simply supported beams at both ends, the distributed load is equal for each length and q is determined as $q = 0.001; 0005; 0.01; 0.05 \ nN/nm$. The point load will be used as a variable in the form of $P = q(L/2) \ nN$ depending on the span.

In cantilever beams, the distributed load is equal for each length and q is determined as $q = 0.001; 0005; 0.01; 0.05 \ nN/nm$. The point load will also be used as a variable in the form of $P = q(L/2) \ nN$ [42].

The abbreviations S-S and C-F refer to the simply supported beam and the cantilever beam. Distributed loads act through the span. The point loads act at the center of the length in the S–S beam and at the free end in the C–F beam. The point loads are selected to create an equal maximum bending effect on the bending effect of the distributed load.

Table 1. Optimal cross-sectional area value (nm^2) for various beam length values L (nm) of beams that are made of CNT–BNNT and have different supporting and loading conditions.

Beam Type and Loading	CNT			BNNT		
	$L = 20$	$L = 40$	$L = 80$	$L = 20$	$L = 40$	$L = 80$
S–S, q = 0.001 nN/nm	0.5000	0.7941	1.5888	0.4674	0.7497	1.4944
S–S, P = 0.0005L nN	0.4580	0.7371	1.4745	0.4178	0.6934	1.3866
C–F, q = 0.001 nN/nm	0.8458	1.6872	3.3738	0.7948	1.5920	3.1759
C–F, P = 0.0005L nN	0.9296	1.8568	3.7134	0.8752	1.7476	3.4950

Table 2. Comparison of the optimal cross-sectional area (nm^2) values for CNT–BNNT beam materials in case of distributed loads and point loads for S–S beams with different lengths.

Loading	Beam Length, nm							
$q, \ nN/nm$	CNT				BNNT			
$P, \ nN$	10	20	40	80	10	20	40	80
q = 0.001	0.1960	0.5000	0.7941	1.5888	0.1960	0.4674	0.7497	1.4944
P = 0.0005L	0.1960	0.4580	0.7371	1.4745	0.1960	0.4178	0.6934	1.3866
q = 0.005	0.4051	0.6794	1.3578	2.7152	0.3698	0.6391	1.2766	2.5546
P = 0.0025L	0.3619	0.6300	1.2605	2.5220	0.3315	0.5944	1.1859	2.3715
q = 0.01	0.5743	0.8568	1.7113	3.4207	0.5227	0.8054	1.6115	3.3248
P = 0.005L	0.5161	0.7959	1.5876	3.1755	0.4675	0.7470	1.4938	2.9892
q = 0.05	0.7319	1.4624	2.9260	14.2334	0.6892	1.3777	2.7541	11.8536
P = 0.025L	0.6792	1.3599	2.7148	11.4045	0.6387	1.2784	2.5555	9.4837

Table 3. A comparison of this study and reference for obtained optimal cross-sectional area (nm^2) results for two different distributed loads on the S–S beams made of CNT.

L (nm)	$q = 0.001 \ nN/nm$		$q = 0.01 \ nN/nm$	
	This Study	Numanoğlu and Nazarov [42]	This Study	Numanoğlu and Nazarov [42]
20	0.5125	0.5127	0.8596	0.8599
30	0.5956	0.5958	1.2825	1.2831
40	0.7938	0.7938	1.7104	1.7100
50	0.9923	0.9925	2.1382	2.1375
75	1.4890	1.4893	3.4074	3.6638

Table 4. Obtained optimal cross-sections, cross-sectional areas, and optimization constraints by applying a distributed load of $q = 0.005 \ nN/m$ to CNT S–S beams with different lengths.

Beam Length	Optimal Area	Optimal Cross-Sect.	Height	Width	Diameter	Max Disp.	Max Stress	Disp. ratio	Stress ratio
L (nm)	A (nm^2)	Rectangle Circle	h (nm)	b (nm)	D (nm)	w_{max} (nm)	σ_{max} (TPa)	$\dfrac{w_{max}}{w_{limit}}$	$\dfrac{\sigma_{max}}{\sigma_{limit}}$
10	0.4067	Circle			0.72	0.0489	0.0016	0.999	0.149
20	0.6794	Rectangle	1.36	0.50		0.0989	0.0015	0.998	0.148
50	1.6966	Rectangle	3.39	0.50		0.2500	0.0015	0.998	0.148
80	2.7166	Rectangle	5.43	0.50		0.3994	0.0015	0.998	0.147
100	3.3935	Rectangle	6.79	0.50		0.4998	0.0016	0.999	0.148

When the contents of tables are compared, the results for distributed and point loads which produce an equal bending effect show that for small lengths, numeric values are in approximate with each other and for large lengths, they are not. As a result, although the bending effects are equal, since the bending responses of the point and distributed loads are different, the results of the optimal cross-sectional area are different.

S–S beams require a more cross-sectional area in case of distributed load, while the C–F beam requires more cross-sectional area in case of point load.

Table 5. Obtained optimal cross-sections, cross-sectional areas, and optimization constraints by applying a distributed load of $q = 0.005\ nN/m$ to CNT C–F beams with different lengths.

Beam Length	Optimal Area	Optimal Cross-Sect.	Height	Width	Diameter	Max Disp.	Max Stress	Disp. ratio	Stress ratio
$L\ (nm)$	$A\ (nm^2)$	*Rectangle* *Circle*	h (nm)	b (nm)	D (nm)	w_{max} (nm)	σ_{max} (TPa)	$\dfrac{w_{max}}{w_{limit}}$	$\dfrac{\sigma_{max}}{\sigma_{limit}}$
10	1.2609	Circle			0.04	0.0494	0.0013	0.988	0.114
20	1.4435	Rectangle	2.88	0.50		0.0997	0.0014	0.998	0.130
50	3.6062	Rectangle	7.21	0.50		0.2498	0.0014	0.999	0.131
80	13.6571	Rectangle	7.50	1.82		0.3999	0.0009	0.999	0.085
100	26.7120	Rectangle	7.50	3.56		0.4992	0.0007	0.998	0.068

Table 6. Obtained optimal cross-sectional values by applying individual load at different values to CNT and BNNT beams.

| Boundary Condition	Loading	Beam length (nm)							
		CNT				BNNT			
		10	20	40	80	10	20	40	80
S–S	P = 1 nN	1.0789	1.7018	2.7164	5.6944	1.0146	1.6099	2.5403	4.7432
	P = 2 nN	1.3594	2.1545	3.4203	11.3921	1.2753	2.0279	3.2180	9.4828
	P = 3 nN	1.5539	2.4687	4.2705	17.0828	1.4622	2.3238	3.6856	14.2323
	P = 4 nN	1.7150	2.7152	5.6939	22.7619	1.6089	2.5549	4.7518	18.9680
	P = 5 nN	1.8483	2.9271	7.1186	28.4534	1.7364	2.7534	5.9369	23.7381
C–F	P = 1 nN	2.7167	5.7012	22.7691	-	2.5552	4.7453	18.9654	-
	P = 2 nN	3.4226	11.4256	-	-	3.2187	9.5069	-	-
	P = 3 nN	4.2670	17.0703	-	-	3.6903	14.2315	-	-
	P = 4 nN	5.6892	22.7635	-	-	4.7453	18.9652	-	-
	P = 5 nN	7.1138	28.4485	-	-	5.9274	23.7082	-	-
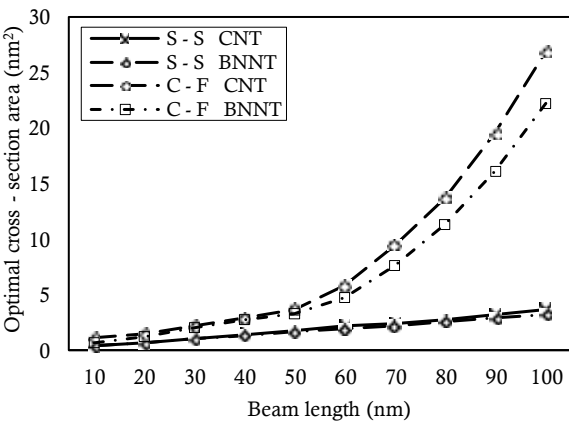
ig. 1. Optimal cross-sectional area values for increasing length values of CNT S–S and C–F beams and BNNT S–S and C–F beams $(q = 0.05\ nN/nm)$.
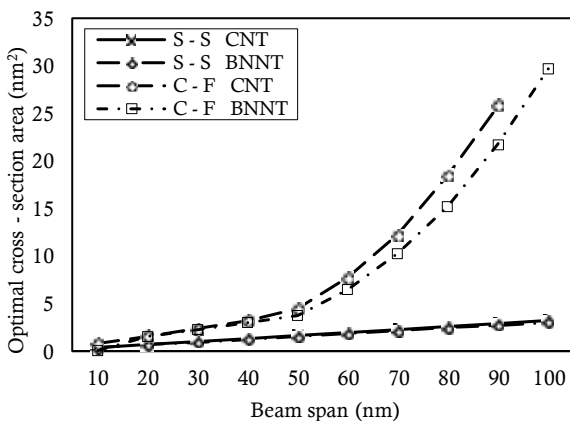

Fig. 2. Optimal cross-sectional area values for increasing length values of CNT S–S and C–F beams and BNNT S–S and C–F beams $(P = 0.025L\ nN)$.
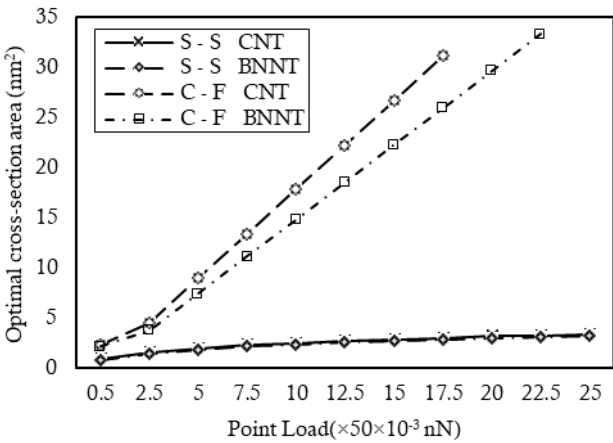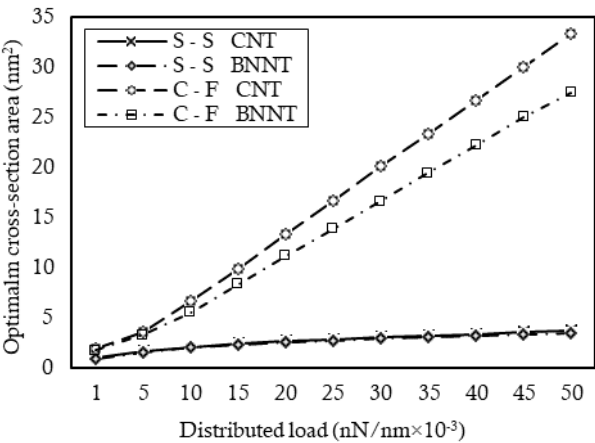

(a)   (b)

Fig. 3. Optimal cross-sectional area values for increasing length values of CNT S–S and C–F beams and BNNT S–S and C–F beams.
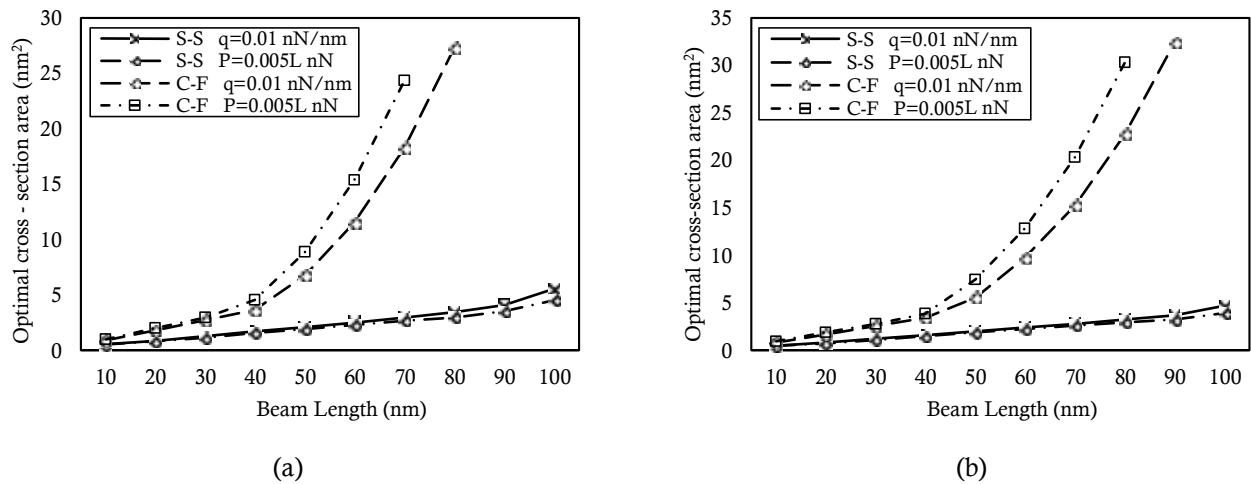
Fig. 4. Optimal cross-sectional area values for increasing length values and different point–distributed load values of CNT S–S and C–F beams and BNNT S–S and C–F beams **a)** CNT **b)** BNNT.
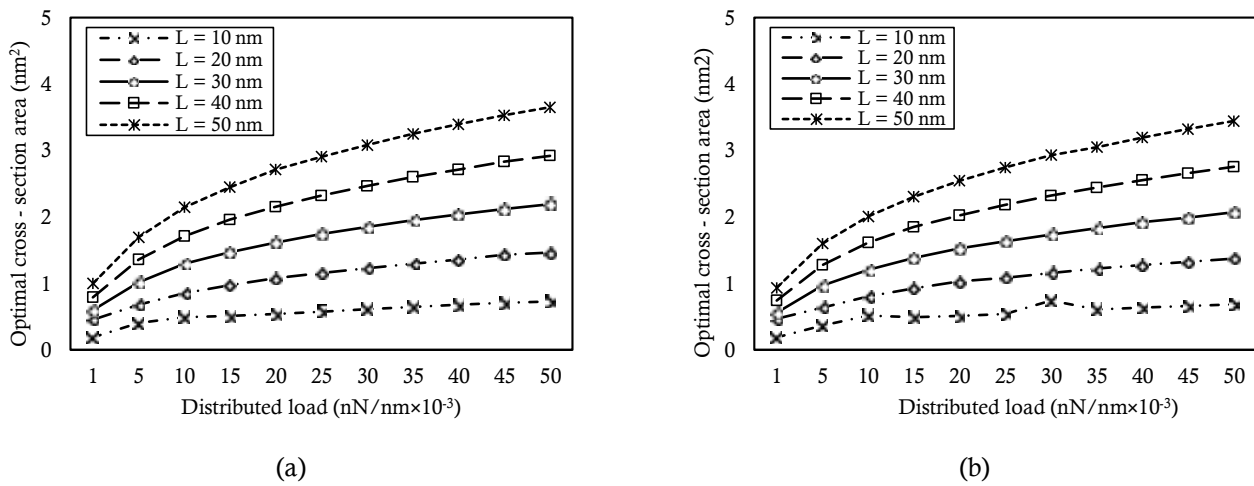

Fig. 5. Optimal cross-sectional area values for increasing distributed load values and different length values of CNT S–S beams and BNNT S–S beams **a)** CNT **b)** BNNT.
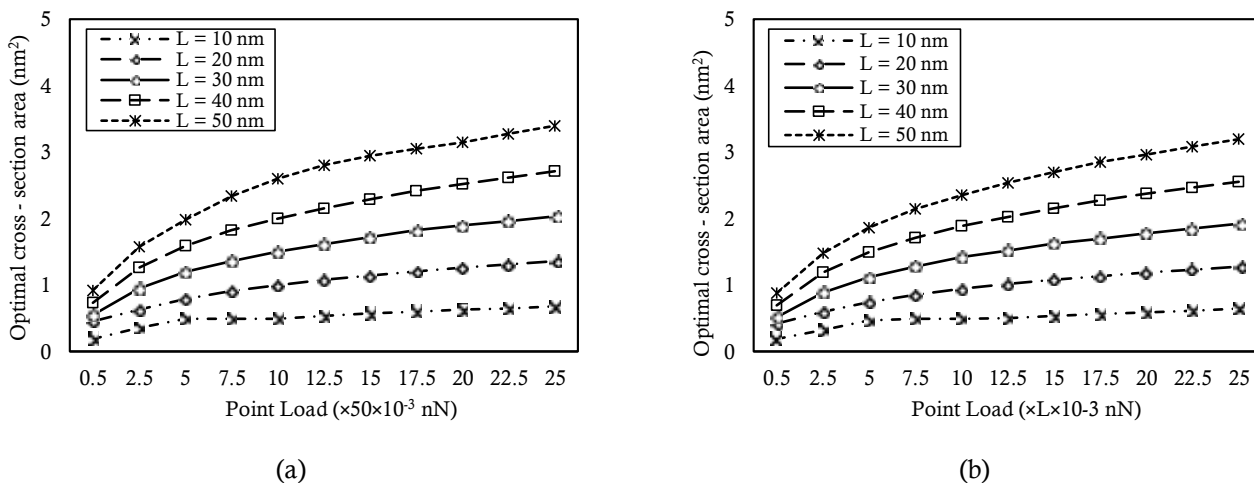

Fig. 6. Optimal cross-sectional area values for point load values selected to give equal bending effect as increasing distributed load and different length values of CNT S–S beams and BNNT S–S beams **a)** CNT **b)** BNNT.

When the tables are examined, it can be seen that CNT results are at lower numerical values compared to BNNT results. The reason for this is the elasticity module which directly affects the displacement. When the data related to C–F beam is examined in the tables, it can be seen that some results are not presented. The reason behind this situation is the optimal cross-sectional areas required by the respective lengths and loads are not included in the previously defined limits.
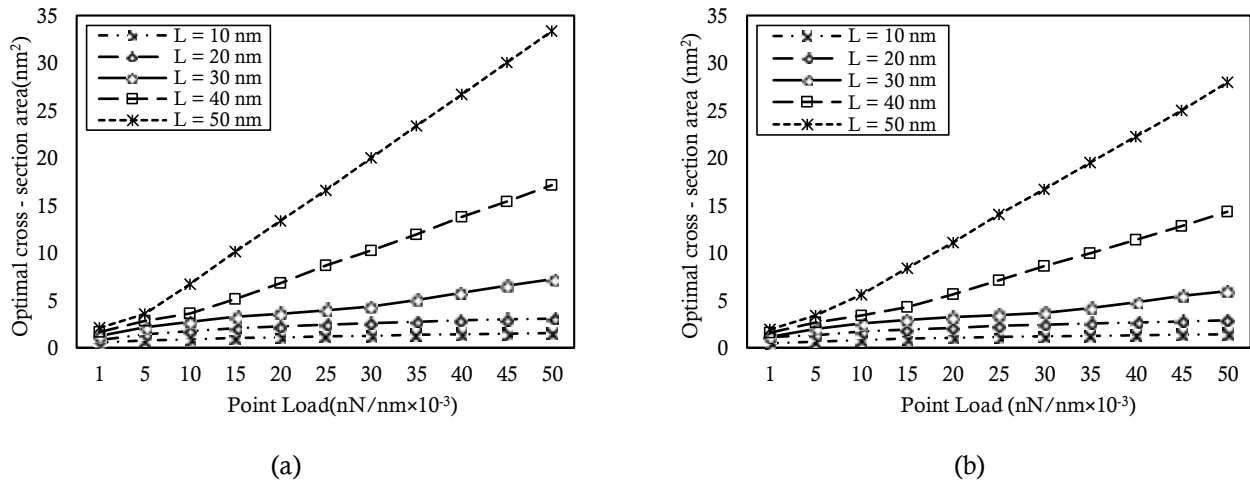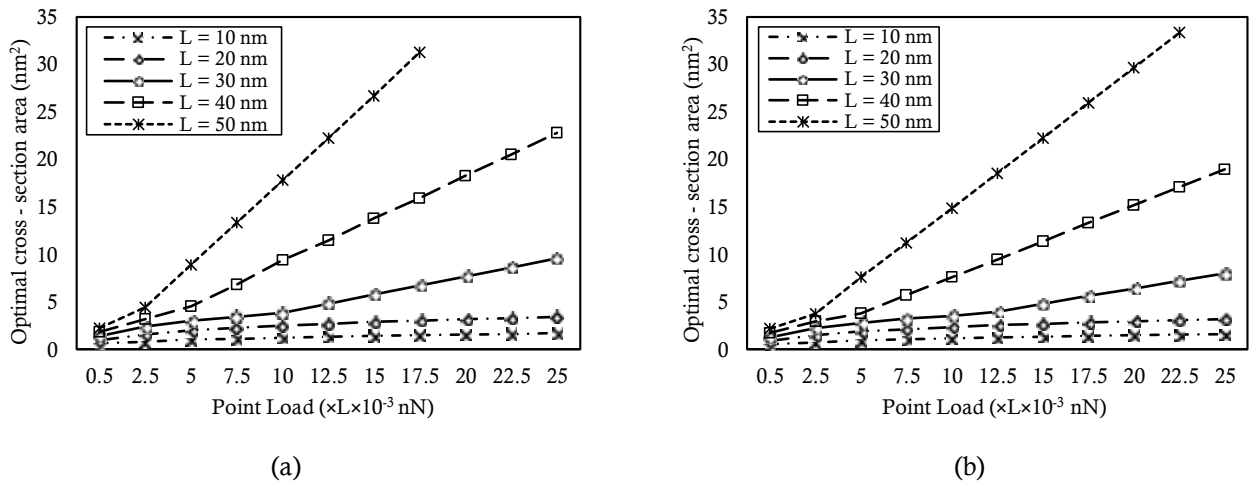
Fig. 7. Optimal cross-sectional area values for increasing distributed load values and different length values of CNT C–F beams and BNNT C–F beams **a)** CNT **b)** BNNT.

Fig. 8. Optimal cross-sectional area values for point load values selected to give equal bending effect as increasing distributed load and different length values of CNT C–F beams and BNNT C–F beams **a)** CNT **b)** BNNT.
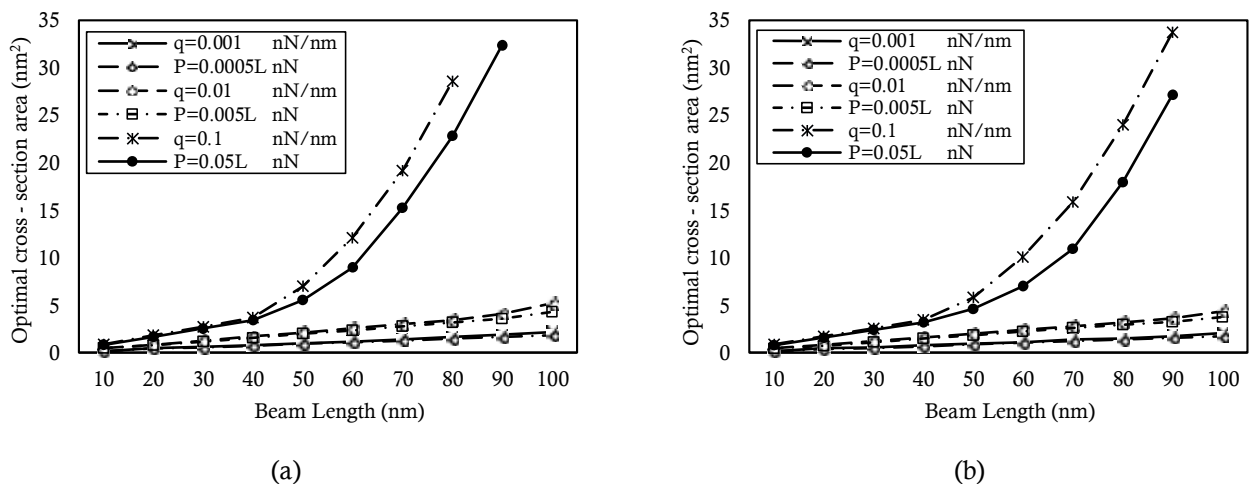

Fig. 9. Obtained optimal cross-sectional area values for CNT S–S beams and BNNT S–S beams which are applied with distributed and singular load pair that gives the equal maximum bending effect with each other **a)** CNT **b)** BNNT.
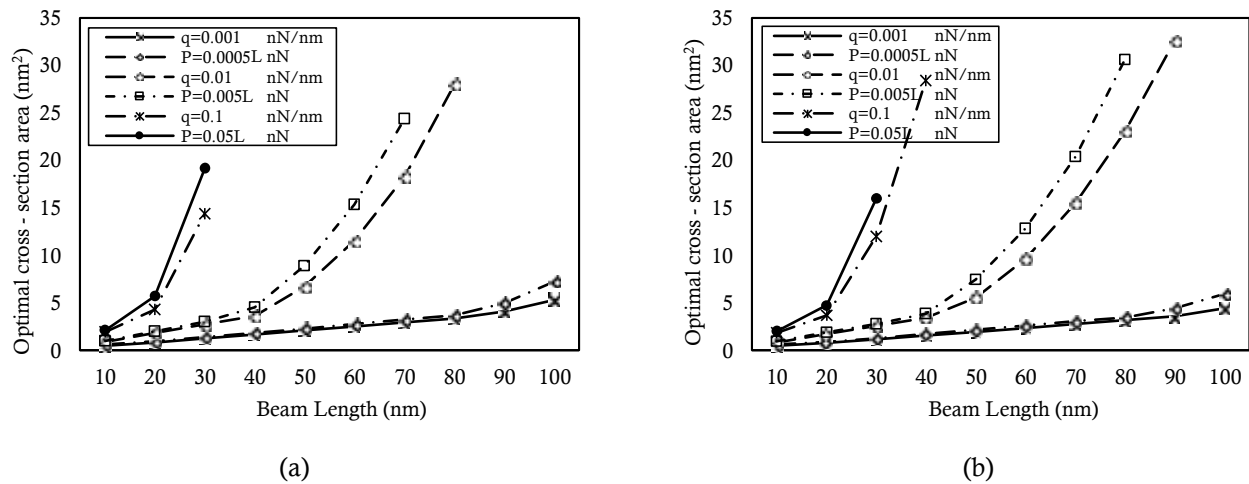
Fig. 10. Obtained optimal cross-sectional area values for CNT C–F beams and BNNT C–F beams which are applied with distributed and singular load pair that gives the equal maximum bending effect with each other **a)** CNT **b)** BNNT.

6. Conclusion

In this study, the deflection behavior of BNNT and CNT beams which have an important position in the developing technologies were investigated by comparing under various loading and supporting conditions. For this investigation, nonlocal elasticity theory which was used for modeling of nano-scale beams were combined with Social Spider Optimization method to achieve the solution. When the obtained solutions were examined, it was seen that cross-sectional area values increase depending on the increase of the length and the loading values. If the results are compared based on the material type, it can be concluded that optimal cross-section values of BNNT beams are less than CNT beam values. The reason for this being the material with a higher elasticity module requiring less cross-sectional area. Also, it was found that the small length values in circular cross-section are more optimal than high length values in rectangular cross-section. Finally, the application of non-local theory to the problem resulted in an increase in optimal cross-section values.

Conflict of Interest

The authors declared no potential conflicts of interest with respect to the research, authorship, and publication of this article.

Funding

The authors received no financial support for the research, authorship, and publication of this article.

Nomenclature

a	Characteristic internal length	Per	Performance of beam design
A	Cross-section area	q	Distributed load
b	Width of rectangular section	u	Motion component
c_i	Integral constants (i= 1, 2, 3, 4)	V	Volume of body
C	Total violation	w	Deflection
C_{klmn}	Fourth-order elasticity tensor	w_j	Weight of the spider
d_{ij}	Euclidean distance between the spiders	w_{limit}	Boundary deflection
D	Diameter of circular section	w_{max}	Maximum deflection
e_0	Nonlocal parameter	x , y	Coordinates
E	Modulus of elasticity	$\bar{\mathbf{x}}$	Design variables vector
f_j	Mass force	α	Nonlocal module
h	Height of rectangular section	ε_{ij}	Strain tensor
I	Moment of inertia	φ	Material constant
L_0	Linear differential operator	λ , μ	Lame constants
l	Characteristic external length	ρ	Mass of unit volume
M_{xx}	Nonlocal internal moment	σ_{ij}	Nonlocal stress

M^c	Classical internal moment	σ_{ij}^c	Classical stress
N_f	Number of female spiders	σ_{limit}	Boundary stress
N_m	Number of male spiders	σ_{max}	Maximum stress

References

[1] Eigler, D.M., Schweizer E.K., Positioning single atoms with a scanning tunneling microscope, *Nature*, 344, 1990, 524–526.

[2] Iijima, S., Helical microtubules of graphitic carbon, *Nature*, 354, 1991, 56-58.

[3] Wang, Q., Wave propagation in carbon nanotubes via nonlocal continuum mechanics, *Journal of Applied Physics*, 98, 2005, 124301.

[4] Civalek, O., Demir, Ç., Akgöz, B. Free vibration and bending analyses of cantilever microtubules based on nonlocal continuum model, *Mathematical and Computational Applications*, 15(2), 2010, 289–298.

[5] Sudak, L.J., Column buckling of multiwalled carbon nanotubes using nonlocal continuum mechanics, *Journal of Applied Physics*, 94, 2003, 7281.

[6] Mercan, K., Civalek, O., DSC method for buckling analysis of boron nitride nanotube (BNNT) surrounded by an elastic matrix, *Composite Structures*, 143, 2016, 300–309.

[7] Civalek O., Demir Ç., Bending analysis of microtubules using nonlocal Euler-Bernoulli beam theory, *Applied Mathematical Modelling*, 35, 2011, 2053–2067.

[8] Yang, X., *Nature-Inspired Metaheuristic Algorithms*, Second Edition, 2010.

[9] Işık, Ç., *Bending and free vibration analysis of nano and microstructures based on nonlocal elasticity theory* (in Turkish), Ms. C. Thesis, Akdeniz University, Antalya, 2011.

[10] Tepe, A., *A study of small scale dimensions of structures in nonlocal elasticity* (in Turkish), Ph. D. Thesis, Istanbul Technical University, İstanbul, 2007.

[11] Eringen, A.C., On differential equations of nonlocal elasticity and solutions of screw dislocation and surface waves, *Journal of Applied Physics*, 54, 1983, 4703.

[12] Reddy, J.N., Pang, S., Nonlocal continuum theories of beams for the analysis of carbon nanotubes, *Journal of Applied Physics*, 103, 2008, 23511.

[13] Cuevas, E., Cienfuegos, M., A new algorithm inspired in the behavior of the social-spider for constrained optimization, *Expert Systems with Applications*, 41, 2014, 412–425.

[14] Akgöz, B., Civalek, Ö., Strain gradient elasticity and modified couple stress models for buckling analysis of axially loaded micro-scaled beams, *International Journal of Engineering Science*, 49, 2011, 1268-1280.

[15] Akgöz, B., Civalek, Ö., Free vibration analysis of axially functionally graded tapered Bernoulli–Euler microbeams based on the modified couple stress theory, *Composite Structures*, 98, 2013, 314-322.

[16] Sedighi, H.M., Size-dependent dynamic pull-in instability of vibrating electrically actuated microbeams based on the strain gradient elasticity theory, *Acta Astronautica*, 95, 2014, 111-123.

[17] Tadi Beni, Y., Size-dependent electromechanical bending, buckling, and free vibration analysis of functionally graded piezoelectric nanobeams, *Journal of Intelligent Material Systems and Structures*, 27, 2016, 2199-2215.

[18] Samani, M.S. E., Beni, Y.T., Size-dependent thermo-mechanical buckling of the flexoelectric nanobeam. *Materials Research Express*, 5, 2018, 085018.

[19] Esmaeili, M., Tadi Beni, Y., Vibration and Buckling Analysis of Functionally Graded Flexoelectric Smart Beam, *Journal of Applied and Computational Mechanics*, 5, 2019, 900-917.

[20] Ebrahimi, F., Barati, M.R., Nonlocal and surface effects on vibration behavior of axially loaded flexoelectric nanobeams subjected to in-plane magnetic field, *Arabian Journal for Science and Engineering*, 43, 2018, 1423-1433.

[21] Akgöz, B., Civalek, Ö., A size-dependent shear deformation beam model based on the strain gradient elasticity theory, *International Journal of Engineering Science*, 70, 2013, 1-14.

[22] Beni, Y.T., Size-dependent analysis of piezoelectric nanobeams including electro-mechanical coupling, *Mechanics Research Communications*, 75, 2016, 67-80.

[23] Sedighi, H.M., Koochi, A., Daneshmand, F., Abadyan, M., Non-linear dynamic instability of a double-sided nano-bridge considering centrifugal force and rarefied gas flow, *International Journal of Non-Linear Mechanics*, 77, 2015, 96-106.

[24] Sedighi, H.M., Bozorgmehri, A., Dynamic instability analysis of doubly clamped cylindrical nanowires in the presence of Casimir attraction and surface effects using modified couple stress theory, *Acta Mechanica*, 227, 2016, 1575-1591.

[25] Ouakad, H. M., Sedighi, H.M., Younis, M.I., One-to-one and three-to-one internal resonances in MEMS shallow arches, *Journal of Computational and Nonlinear Dynamics*, 12, 2017, 051025.

[26] Koochi, A., Sedighi, H.M., Abadyan, M., Modeling the size-dependent pull-in instability of beam-type NEMS using strain gradient theory, *Latin American Journal of Solids and Structures*, 11, 2014, 1806-1829.

[27] Sedighi, H.M., Chan-Gizian, M., Noghreha-Badi, A., Dynamic pull-in instability of geometrically nonlinear actuated micro-beams based on the modified couple stress theory, *Latin American Journal of Solids and Structures*, 11, 2014 810-825.

[28] Cuevas, E., Cienfuegos, M., Rojas, R., Padilla, A., A Computational Intelligence Optimization Algorithm Based on

the Behavior of the Social-Spider, in *Computational Intelligence Applications in Modeling and Control*, Editors: Azar, A.T., Vaidyanathan, S., Springer, 2015, 123–146.

[29] Aydogdu, I., Comparison of metaheuristics on multi-objective (Cost&C02) optimization of RC cantilever retaining walls, *Pamukkale University Journal of Engineering Sciences*, 23(3), 2016, 221–231.

[30] Aydogdu, I., Carbas, S., and Akin, A. Effect of Levy flight on the discrete optimum design of steel skeletal structures using metaheuristics, *Steel and Composite Structures*, 24(1), 2017, 93–112.

[31] Saka, M.P., Carbas, S., Aydogdu, I., Akin, A., Geem, Z.W., Comparative study on recent metaheuristic algorithms in design optimization of cold-formed steel structures, in *Engineering and Applied Sciences Optimization*, Editors: Lazaros, N.D., Papadrakakis, M., 2015, Springer, 145-173.

[32] Saka, M.P., Carbas, S., Aydogdu, I., Akin, A., Use of swarm intelligence in structural steel design optimization, in *Metaheuristics and Optimization in Civil Engineering*, Springer, Editors: Yang, X.-S. Bekdas, G., Nigdeli, S.N., Springer, 2016, 43-73.

[33] Cuevas, E., Cienfuegos, M., Zaldivar, D., Perez-Cisneros, M., A swarm optimization algorithm inspired in the behavior of the social-spider, *Expert Systems with Applications*, 40(16), 2013, 6374-6384.

[34] Yu, J.J.Q., Li, V.O.K., A social spider algorithm for global optimization, *Applied Soft Computing*, 30, 2015, 614-627.

[35] Cuevas, E., Cortés, M.A.D., Navarro, D.A.O., Social-Spider Algorithm for Constrained Optimization, in *Advances of Evolutionary Computation: Methods and Operators*, Springer, 2016, 175-202.

[36] Esapour, K., Hoseinzadeh, R., Akbari-Zadeh, M.-R., A new sufficient method based on levy-social spider technique for optimal economic dispatch of thermal power unit, *Journal of Intelligent & Fuzzy Systems*, 28(3), 2015, 1137-1143.

[37] Kavousi-Fard, A., Abbasi, A., Rostami, M.-A., Khosravi, A., Optimal distribution feeder reconfiguration for increasing the penetration of plug-in electric vehicles and minimizing network costs, *Energy*, 93, 2015, 1693-1703.

[38] Yu, J.J.Q. and Li, V.O.K. A social spider algorithm for solving the non-convex economic load dispatch problem, *Neurocomputing*, 171, 2016, 955-965.

[39] Aydogdu, I., Efe, P., Yetkin, M., Akn, A., Optimum design of steel space structures using social spider optimization algorithm with spider jump technique, *Structural Engineering and Mechanics*, 62, 2017, 259-272.

[40] Pereira, D.R., Pazoti, M.A., Pereira, L.A.M., Rodrigues, D., Ramos, C.O., Souza, A.N., Papa, J.P., Social-spider optimization-based support vector machines applied for energy theft detection, *Computers & Electrical Engineering*, 49, 2016, 25-38.

[41] Akin, A., Aydogdu, I., Bilir, T., Cost and CO 2 optimization for RC short column sections subjected to axial load and uniaxial/biaxial bending using the social spider optimization algorithm, *Sustainable Construction Materials and Technologies 4*, Las Vegas, USA, 2016, 293-303.

[42] Numanoglu, H.M., Nazarov, V., The beam model and optimum design of carbon nanotubes under stress and displacement conditions (in Turkish), TUBITAK 2209–A Project, 1919B011503317, 2017.

[43] Wiecha, P. R., Evolutionary multi-objective optimization of color pixels based on dielectric nanoantennas, *Nature Nanotechnology*, 12, 2017, 163-170.

[44] Ozbay, E., Plasmonics: Merging photonics and electronics at nanoscale dimensions, *Science*, 311, 2006, 189-193.

ORCID iD

Büşra Uzun https://orcid.org/ 0000-0002-7636-7170
Ömer Civalek https://orcid.org/0000-0003-1907-9479
Ibrahim Aydogdu https://orcid.org/0000-0002-8281-2365

Publisher's Note Shahid Chamran University of Ahvaz remains neutral with regard to jurisdictional claims in published maps and institutional affiliations.